Appendix A

A1 Methodology

Samples were prepared by trimming off weathered surfaces using a rock saw. Melanosome was removed from migmatite samples. The remaining material was washed in water and crushed. A ~10 g aliquot per sample was powdered using a tungsten carbide ring mill for bulk-rock geochemistry. Zircon, pyrite, and garnet crystals were extracted using standard separation techniques (Jasper Canyon shaking table, Frantz magnetic separation, heavy liquids [lithium heteropolytungstates and diiodomethane]). Hand-picked zircon and pyrite crystals were mounted in epoxy resin and polished to approximately half grain thickness to expose an interior cross section through the individual crystals. Grains were mounted within a 5 mm radius from the centre of a 25 mm diameter epoxy resin disk for SIMS analysis. The polished mounts were cleaned in an ultrasonic bath in multiple steps using isopropanol, ethanol, soap solution, and deionized water. Subsequently, the mounts were dried in an oven for ~24 hrs at 60°C. A 40 nm gold coat was applied to the mount surface. To reveal internal growth structures, CL images of zircon grains were taken prior to SIMS analysis using a Tescan MIRA3 field emission scanning electron microscope. SIMS U-Pb and oxygen isotope analyses were located on the same zircon growth zone (see supplementary Figure A2). Magmatic rims of zircon grains were targeted for SIMS analyses to avoid inherited older growth zones. SIMS U-Pb analysis was conducted subsequent to SIMS oxygen isotope analysis. Backscatter electron (BSE) images and energy dispersive X-ray analysis (EDX) of pyrite grains were obtained prior to SIMS analysis using a Hitachi TM3030 tabletop scanning electron microscope (SEM) coupled with a SwfitED3000 EDX spectrometer. Field Emission Scanning Electron Microscope (FESEM) element maps and BSE images of garnet grains were obtained using a Tescan Integrated Mineral Analyzer (TIMA). The mineralogy of the samples was studied in thin section using a polarized light microscope. CL and BSE imaging, EDX analysis, and element mapping was conducted using the facilities of the John de Laeter Centre, Curtin University, Western Australia.

A1.1 SIMS zircon oxygen and pyrite sulfur isotope ratios

Oxygen and sulfur isotope analysis were conducted on a CAMECA IMS 1280 secondary ion mass spectrometer (SIMS) at the Centre for Microscopy, Characterisation, and Analysis (CMCA) at the University of Western Australia and at the Guangzhou Institute of Geochemistry (GIG), Chinese Academy of Sciences, China. Analytical methods have been described in detail by Yang et al. (2018) for oxygen isotope analysis and by LaFlamme et al. (2016) for sulfur isotope analysis. A Cs^+ primary ion beam was accelerated at 10 keV with an intensity of 2–3 nA. The spot diameter was ~10–15 µm. Prior to analysis, each site was pre-sputtered for 30-35 s to remove the Au-coat in a ~20 μm^2 area. Secondary optics were centered automatically before each analysis.

Oxygen and sulfur isotope compositions are reported in the conventional delta notation; expressed as $\delta^{18}O$ and $\delta^{3x}S$, respectively. The delta notation reflects the permil deviation in the isotope ratio of the sample ($^{18}O/^{16}O$, $^{34}S/^{32}S$, and $^{33}S/^{32}S$ in this case) relative to a reference material. Reference materials are standard mean ocean water (VSMOW) (Baertschi, 1976) for $\delta^{18}O$, and the Cañon Diabolo Troilite (VCDT) (Ding et al., 2001) for $\delta^{34}S$ and $\delta^{33}S$. The triple sulfur isotopic composition of pyrite is expressed as $\Delta^{33}S$, defined as $\delta^{33}S$-1000*((1+$\delta^{34}S$/1000)^0.515-1).

For zircon oxygen isotope analysis, the ^{18}O and ^{16}O ions were detected simultaneously by two faraday cups. Instrumental mass fractionation and drift were determined through

repetitive analyses of zircon standard 91500 ($\delta^{18}O$ = 9.9±0.6‰) (Wiedenbeck et al., 2004). Zircon reference materials Temora-2 ($\delta^{18}O$ = 8.2±0.03‰) (Black et al., 2004), and Penglai ($\delta^{18}O$ = 5.31±0.1‰) (Li et al., 2010) were used as a secondary reference to monitor the quality of the applied corrections. The analysis of the secondary standard Temora-2 yielded $\delta^{18}O$ of 8.0 ± 0.5‰, and 7.8 ± 0.4‰ (2σ) in accordance with the accepted value (but see Schmitt et al. (2019) for a discussion of oxygen isotopic heterogeneity in different batches of Temora-2). The analysis of the secondary standard Penglai yielded $\delta^{18}O$ of 5.0 ± 0.3‰ (2σ) in accordance with the accepted value. Repeat analyses of the primary standard indicate a repeatability of ≤0.2‰ (1σ) for all runs. To ensure that the oxygen isotope values reflect a primary signature, the zircon OH-content, an indicator of secondary alteration (Pidgeon et al., 2017; Liebmann et al., 2021b) was determined qualitatively as compared to reference zircon 91500 (see supplementary Figure A7) for all but six samples. Zircon mounts were held under vacuum for at least 3 days prior to this analysis. Zircon OH is reported as OH/O, determined as counts of $^{16}O^{1}H$ over counts of ^{16}O.

For pyrite sulfur isotope analysis, the ^{34}S, ^{33}S, and ^{32}S ions were detected simultaneously by three faraday cups. Instrumental mass fractionation and drift were determined through repeated analyses of pyrite standard Sierra ($\delta^{34}S$ = 2.17 ± 0.28‰, $\Delta^{33}S$ = -0.02 ± 0.01‰) (LaFlamme et al., 2016). Pyrite standards Ruttan ($\delta^{34}S$= 1.2 ± 0.35‰, $\Delta^{33}S$ = 0 ± 0.22‰) (Crowe and Vaughan, 1996) and Balmat ($\delta^{34}S$ = 16.02 ± 1.18‰, $\Delta^{33}S$ = 0 ± 0.23‰) (Whitehouse, 2013) were used as secondary standards to monitor the quality of the applied corrections. The analysis of Ruttan pyrite yielded $\delta^{34}S$ of 1.2 ± 0.3‰, and $\Delta^{33}S$ of -0.01 ± 0.08‰; the analysis of Balmat pyrite yielded $\delta^{34}S$ of 16.3 ± 0.2‰, and $\Delta^{33}S$ of -0.03 ± 0.08‰ (2σ) in accordance with the accepted values. Repeat analyses of the primary standard indicate a repeatability of ≤ 0.15‰ (1σ) for $\delta^{34}S$ and ≤ 0.04‰ (1σ) for $\Delta^{33}S$ for all runs (Supplementary Table A4).

Oxygen and sulfur isotope measurement results and field centering values of reference materials are given in supplementary Figure A7, and supplementary Tables A3 and A4. Images of representative zircon and pyrite grains are given in supplementary Figures A2 and A3.

A1.1. Error propagation for SIMS analyses

The uncertainty of individual analyses can be estimated through propagation of uncertainty. The propagated error of an individual analysis considering the internal uncertainty and the uncertainty associated with the correction for instrumental drift is given by:

$$\sigma_{R_{dc}} = \sqrt{\sigma_i^2 + \sigma_{reg}^2} \qquad \textit{Eq. 1}$$

Where σ_i is the internal precision and σ_{reg} is the standard error of the linear least square regression to model instrumental drift, given by:

$$\sigma_{reg} = \sqrt{x^2\sigma_m^2 + \sigma_c^2 + 2x\rho\sigma_m\sigma_c} \qquad \textit{Eq. 2}$$

Where σ_m and σ_c are the standard errors associated with respectively slope and y-intercept of the linear regression model, ρ is the correlation coefficient, and x is the analysis number.

The uncertainty related to estimating instrumental mass fractionation α can be calculated as:

$$\sigma_\alpha = \sqrt{\left(\frac{\sigma_{R\ std}}{R_{acc\ std}}\right)^2 + \left(\frac{\overline{R_{std}} * \sigma_{R_{acc\ std}}}{{R_{acc\ std}}^2}\right)^2} \quad \textit{Eq. 3}$$

Where $\sigma_{R\ std}$ is the standard deviation of the measured isotope ratio of the primary working reference material, $R_{acc\ std}$ is the accepted isotope ratio of the primary working reference material, $\overline{R_{std}}$ is the mean of the measured isotope ratio of the primary working reference material, and $\sigma_{R_{acc\ std}}$ is the uncertainty of the accepted isotope ratio of the primary working reference material. The propagated uncertainty of individual $\delta^{18}O$ and $\delta^{x}S$ values considering the uncertainties related to the corrections for instrumental drift and fractionation can be calculated as:

$$\sigma_{\delta^x X} = \sqrt{\left(\frac{1000 * \sigma_{Rdc}}{\alpha * R_{ref}}\right)^2 + \left(\frac{R_{unk} * \sigma_\alpha}{\alpha}\right)^2} \quad \textit{Eq. 4}$$

The uncertainty of individual $\Delta^{33}S$ values $\sigma_{\Delta 33S}$ is calculated as:

$$\sigma_{\Delta 33S} = \sqrt{\left(-0.515 * \sigma_{\delta^{34}S}\left(1+\frac{\delta^{34}S}{1000}\right)^{-0.485}\right)^2 + {\sigma_{\delta^{33}S}}^2 + 2 * cov_{33-34} * \left(-0.515 * \sigma_{\delta^{34}S}\left(1+\frac{\delta^{34}S}{1000}\right)^{-0.485}\right)} \quad \textit{Eq. 5}$$

Where cov_{33-34} is the covariance between $\delta^{34}S$ and $\delta^{33}S$ of the primary reference material.

A1.2 Laser fluorination oxygen isotope geochemistry

Garnet grains were handpicked under a binocular to ensure they were free of inclusions and alteration. Approximately 1.6-1.8 mg of garnet was used per analysis. Laser fluorination oxygen isotope analysis was conducted at the California Institute of Technology using a CO_2 laser with BrF_5 as fluorinating agent following the procedure described by (Sharp, 1990; Valley et al., 1995). All samples were analyzed in duplicate and yielded $\delta^{18}O$ within 0.01-0.36‰ of the replicate for each sample. Six to seven measurements per analytical session of Gore mountain garnet (UWG-2) (Valley et al., 1995) were interspersed with measurements of the unknowns. The analyses of UWG-2 indicate a precision of ≤ 0.07‰ (1σ) for all runs. Delta values are reported as weighted means with 2σ errors unless stated otherwise. Garnet of all samples is almandine-rich with varying spessartine component and occurs as euhedral to subhedral grains (supplementary Figures A5 and A6).

A1.3 SIMS zircon U-Pb geochronology

For eight samples of this study zircon U-Pb ages were obtained using an A.S.I. SHRIMP II sensitive high-resolution ion microprobe at the John de Laeter Centre, Curtin University, Western Australia. Operating procedures are described in detail by (Wingate and Kirkland, 2015). Zircon reference materials Temora-2 (417 ± 2 Ma, 130 ± 21 U ppm; Black et al., 2004), 91500 (1065 ± 1 Ma, 81 ± 5 U ppm; Wiedenbeck et al., 2004), and OG1 (3465 ± 0.6 Ma, 163 ± 48 U ppm; Stern et al., 2009) were used for U-Pb standardization, U concentration, and Pb-Pb referencing, respectively. Secondary reference material OG1

yielded weighted mean $^{207}Pb/^{206}Pb^*$ ages of 3452 ± 35 Ma (MSWD=0.6; n=4), and 3470 ± 13 Ma (MSWD=0.47; n=6); and 91500 yielded a $^{238}U/^{206}Pb^*$ age of 1078 ± 31 Ma (MSWD=0.68, n=5) within uncertainty of the accepted values. Details of calibration and instrumental uncertainties can be found in the supplementary Table A1. An acceleration voltage of 10 keV was used to direct a 15-20 μm diameter primary beam of O_2^- ions onto the zircon grain to sputter secondary ions from its surface. Secondary ions were accelerated to 10 keV into a magnetic field that directs the secondary ion beam into an electron multiplier. During each run the magnetic field was cycled several times to count the secondary ions of eight different mass species and to determine the background. The measured isotopic masses were 196 (species $[^{90}Zr_2{}^{16}O]^+$, count time 2 s), 204 ($^{204}Pb^+$,10 s), 204.1 (background, 10 s), 206 ($^{206}Pb^+$, 10 s), 207($^{207}Pb^+$, 20–40 s), 208 ($^{208}Pb^+$, 10 s), 238 ($^{238}U^+$, 5 s), 248 ($[^{232}Th^{16}O]^+$, 5 s), and 254 ($[^{238}U^{16}O]^+$, 2 s). This cycle was repeated six times for each analysis. Prior to analysis, the primary ion beam was rastered over each site for 2-3 minutes to clean the area.

Raw data were reduced using the Microsoft Excel add-ins SQUID 2.50 and Isoplot 3.75 with the decay constants of Steiger and Jäger (1977). Measured $^{206}Pb^+/^{238}U^+$ ratios are calibrated to the accepted $^{206}Pb/^{238}U$ ratio of the zircon standard, using a calibration curve of $\ln(^{206}Pb^+/^{238}U^+)$ vs. $\ln(UO^+/U^+)$ with a fixed slope of 2.0 (Claoue-Long et al., 1995). Measured compositions were corrected for the presence of common Pb using measured $^{204}Pb/^{206}Pb$ and the contemporaneous Pb isotopic composition determined according to the terrestrial Pb model of Stacey and Kramers (1975). To confirm that common Pb is mainly inherited to the zircon grain rather than related to surface contamination, counts for $^{204}Pb^+$ were monitored during each analysis to ensure that they remained low (≤ 5 counts/10 s for most grains) over the analysis time of ~16 min. Calculated mean ages are quoted in the text at the 2σ level (unless stated otherwise) and include propagated internal and external uncertainty components. No $^{207}Pb/^{206}Pb$ fractionation correction was deemed necessary as OG1 yielded weighted mean $^{207}Pb/^{206}Pb^*$ ages of 3452 ± 35 Ma (MSWD=0.6; n=4), and 3470 ± 13 Ma (MSWD=0.47; n=6) within uncertainty of the accepted value.

2.2.4 LA ICP-MS zircon U-Pb geochronology

For one sample of this study (sample 15K-2) U-Pb isotopic data were collected by laser ablation inductively coupled plasma mass spectrometry (LA ICP-MS) at the GeoHistory Facility, John de Laeter Centre, Curtin University. Zircon was ablated using a Resonetics RESOlution M–50A–LR system, incorporating a COMPex 102–193 nm excimer UV laser coupled to an Agilent 8900 QQQ mass spectrometer. Following two cleaning pulses and a 30 s period of background analysis, samples were spot ablated for 30 s at a 5 Hz repetition rate using a 38 μm beam and laser energy at the sample surface of 2 J/cm^2. An additional 15 s of baseline was collected after ablation. The sample cell was flushed with ultrahigh purity He (300 mL min^{-1}) and N_2 (1.0 mL min^{-1}) and high purity Ar was employed as the plasma carrier gas (flow rate 0.98 L min^{-1}). The time-resolved mass spectra were reduced using the U–Pb geochronology data reduction schemes in Iolite 3.7^{TM} (Paton et al., 2011) with final ages calculated using Isoplot. Zircon standard OG1 (3465 ± 0.6 Ma) (Stern et al., 2009) was used as a primary reference material. Secondary zircon standards yielded weighted mean ages within uncertainty of their accepted values (see supplementary Table A2).

2.2.5 XRF bulk-rock geochemistry

Bulk-rock major and trace element concentrations of 12 samples of this study were determined using a Panalytical Zetium 4 kW X-ray fluorescence spectrometer (XRF) at the California Institute of Technology, USA. Powdered samples were dried at 110°C overnight. Dried powders were then sintered at 1050°C for one hour and loss on ignition (L.O.I) was

determined subsequently. After re-homogenizing sample powders with an agate mortar and pestle, sample powders were fused into glass beads at a flux to sample ratio of 10:1 using a di-lithium tetraborate-lithium metaborate flux. The concentrations of 10 major and 18 trace elements in the samples were measured by comparing their X-ray intensities to those obtained from standards beads. Full analytical methods and uncertainties are given in (Bucholz and Spencer, 2019).

2.2.6 ICP-MS bulk-rock geochemistry

Bulk-rock major element concentrations of one sample (15K-2) was determined in solution by ICP-MS analysis at Bureau Veritas Minerals, Canada. Approximately 0.25 g of sample material was dissolved through multi-acid digestion (HNO_3-$HClO_4$-HF). Subsequently, the solution was dried down, and the residue was dissolved in HCl prior to analysis.

A2 Zircon U-Pb geochronology

In the following the interpretation of zircon U-Pb geochronological data is described in detail. With the exception of sample 15K-2, U-Pb geochronological data was obtained by SIMS analysis. For sample 15K-2 U-Pb ages were obtained by LA-ICP-MS analysis. U-Pb ages are reported with 2σ uncertainty unless stated otherwise. Single spot results are given in supplementary Table B1. Concordia diagrams are shown in Figure 1.

A2.1 Sample 17FIN02

Sample 17FIN02 is a migmatite with medium-grained, garnet-bearing leucosome. Zircon isolated from the leucosome is subhedral, purple in color, and up to 250 µm long. CL images reveal complex or oscillatory zoning, in some grains overgrown by a up to 20 µm thick, homogenous to weakly zoned, low CL response rim. A total of six single spot analyses was on six zircon grains was obtained for sample 17IN02. One analysis was omitted due to high common Pb content. Four of the remaining five analyses are located on zircon rims. They are concordant to normally discordant (1 to 15% discordant) and define a discordia with an upper intercept age of 1896 ± 26 Ma (n=4, MSWD=0.23) which is interpreted as the magmatic crystallization age of the leucosome. One analysis on an older zircon growth zone yields a $^{207}Pb/^{206}Pb^*$ age of 2756 ± 24 Ma (1σ), and is interpreted to date an inherited component.

A2.2 Sample 17FIN03B

Sample 17FIN03B is a migmatite with medium-grained, garnet-bearing leucosome. Zircon isolated from the leucosome is subhedral, brown in color, and up to 200 µm long. CL images reveal low CL response zircon cores overgrown by higher CL response rims with no to weak indication of oscillatory growth pattern. A total of eight single spot analyses on rims of eight zircon grains was obtained for sample 17FIN03B. Two analyses were omitted due to high common lead content (n=2) or due the spot being located on a crack in the zircon grain (n=1). The remaining five analyses are concordant (≤3% discordant). They yield a weighted mean $^{207}Pb/^{206}Pb^*$ age of 1824 ± 13 Ma (n=5, MSWD=0.67), which is interpreted as the magmatic crystallization age of the leucosome.

A2.3 Sample 17FIN05B

Sample 17FIN05B is a migmatite with coarse-grained, garnet-bearing leucosome. Zircon isolated from the leucosome is subhedral, brown in color, and up to 300 µm long. CL images reveal complex or blurred zircon growth patterns overgrown by homogenous to weakly zoned, up to 40 µm thick, low CL response rims. In some cases the growth pattern of the core is truncated by the rims implying that the cores underwent physical abrasion before rim overgrowth. A total of eight single spot analyses on rims of eight zircon grains was obtained

for sample 17FIN05B. Two analyses were omitted due to high common Pb content. All of the remaining six analyses are concordant (<9% discordant) and yield a weighted mean $^{207}Pb/^{206}Pb^*$ age of 1837 ± 9 Ma (n=6, MSWD=0.75) which is interpreted as the magmatic crystallization age of the leucosome.

A2.4 Sample 17FIN06

Sample 17FIN06 is a migmatite with medium-grained, garnet-bearing leucosome. Zircon isolated from the leucosome is subhedral, brown in color, and up to 500 µm long. CL images reveal two types of cores: type I with oscillatory zoning, and type II with low CL response, and homogenous. Zircon cores are overgrown by homogenous to weakly zoned, up to 30 µm thick rims. A total of eight single spot analyses on rims of eight zircon grains was obtained for sample 17FIN06. All of the analyses are concordant (<7% discordant) and yield a concordia age of 1815 ± 16 Ma (n=8, MSWD (of concordance and equivalence)=1.8) which is interpreted as the magmatic crystallization age of the leucosome.

A2.5 Sample 19GH9

Sample 19GH9 is a biotite-muscovite granite. Zircon isolated from this sample is eubhedral, colorless, and up to 300 µm long. CL images reveal ubiquitous oscillatory zoning. A total of seven single spot analyses on five zircon grains was obtained for sample 19GH9. One analysis was omitted due to high common Pb content. The remaining analyses are concordant to normally discordant. Analyses that are <9% discordant yield a weighted mean $^{207}Pb/^{206}Pb^*$ age of 2183 ± 14 Ma (n=5, MSWD=0.2) which is interpreted as the magmatic crystallization age of the granite. One normally discordant analysis (12% discordant) is interpreted to reflect recent Pb loss and was omitted from the calculation of the crystallization age.

A2.6 Sample 19GH11B

Sample 19GH11B is a biotite-muscovite granite. Zircon isolated from this sample is eubhedral, colorless, and up to 400 µm long. CL images reveal ubiquitous oscillatory zoning. A total of seven single spot analyses on three zircon grains was obtained for sample 19GH11B. One analyses overlaps with a crack in the zircon grain and was therefore omitted. The remaining six analyses are concordant to normally discordant and define a discordia with an upper intercept age of 2188 ± 20 Ma (n=6, MSWD=1.5) which is interpreted as the magmatic crystallization age of the granite.

A2.7 Sample CO-17-8

Sample CO-17-8 is a biotite-muscovite granite. Zircon isolated from this sample is euhedral, colorless, and up to 250 µm long. CL images reveal ubiquitous oscillatory zoning. A total of six single spot analyses on rims of six zircon grains was obtained for sample CO-17-8. They are concordant to normally or reversely discordant. The four most concordant analyses (≤11% discordant) yield a weighted mean $^{207}Pb/^{206}Pb^*$ age of 1447 ± 50 Ma (n=4, MSWD=2.0) which is interpreted as the magmatic crystallization age of the granite. The remaining two discordant analyses are interpreted to reflect recent Pb loss. However, they do not define a meaningful discordia together with the other data (MSWD > 3) and are therefore not considered for the calculation of the crystallization age.

A2.8 Sample SP-16-2b

Sample SP-16-2b is a biotite-muscovite granite. Zircon isolated from this sample is subhedral to anhedral, brown in color, and up to 70 µm long. CL images reveal oscillatory zoning. A total of four single spot analyses on four zircon grains was obtained for sample SP-16-2b. One analysis was omitted due to a high common Pb content. The remaining three analyses

are concordant to normally discordant and define a discordia with an upper intercept age of 2664 ± 45 Ma (n=3, MSWD=0.21) which is interpreted as the magmatic crystallization age of the granite.

A2.9 Samples SP-16-22, SP-16-20a, and SP-16-34

Sample SP-16-22 is a biotite-muscovite granite. Zircon isolated from this sample is eubhedral to subhedral, brown in color, and up to 200 μm long. CL images reveal ubiquitous oscillatory zoning. A total of four single spot analyses on three zircon grains was obtained for sample SP-16-22. One analysis was omitted due to a high common Pb content. The remaining three analyses are normally discordant and define a discordia with an upper intercept age of 2654 ± 24 Ma (n=3, MSWD=0.19) which is interpreted as the magmatic crystallization age of the granite. Samples SP-16-20a, and SP-16-34 were collected from the same batholith as sample SP-16-22. Therefore all three samples likely have the same crystallization age of 2654 ± 24 Ma.

A2.10 Sample 15K-2

Sample 15K-2 is a biotite granite. Zircon isolated from this sample is subhedral, colorless, and up to 300 μm long. CL images reveal complex or blurred growth patterns in zircon cores and homogenous to oscillatory zoned rims. A total of 13 single spot analyses on 13 zircon grains was obtained for sample 15K-2. The analyses are concordant to normally or reversely discordant. Analyses that are less than 10% discordant yield a weighted mean $^{207}Pb/^{206}Pb$ age of 2144 ± 28 Ma (n=12, MSWD=0.21), which is interpreted as the magmatic crystallization age of the granite. One normally discordant analysis (13% discordant) is interpreted to reflect recent Pb loss and was omitted from the calculation of the crystallization age.

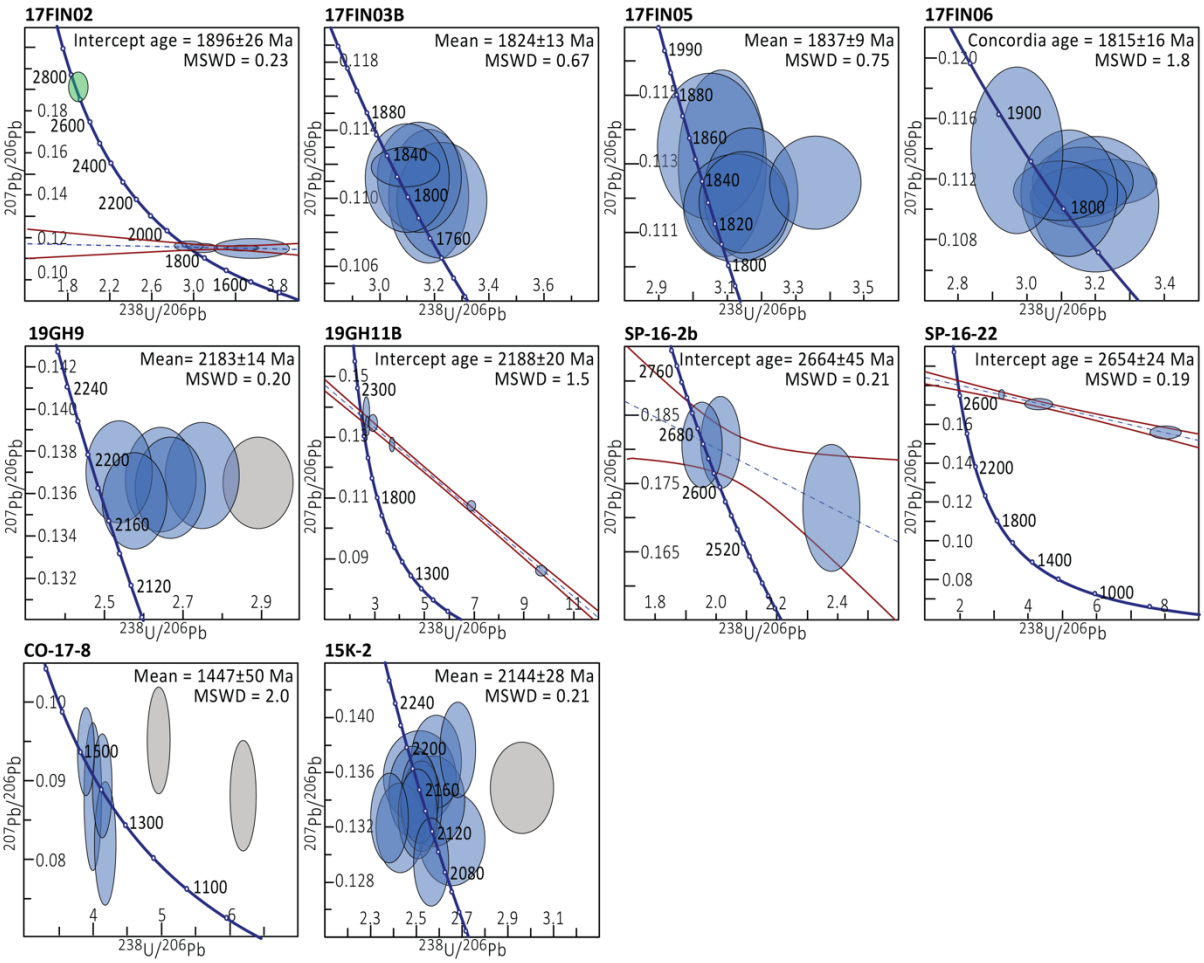

Supplementary Figure A1. Concordia diagrams. Data point error ellipses are shown at 2σ level. Mean ages are weighted mean $^{207}Pb/^{206}Pb^*$ ages. MSWD of concordia age is that of concordance and equivalence. Single spot analyses interpreted as dating magmatic components are shown as blue ellipses, those dating inherited components are shown as green ellipses. Single spot analyses shown as grey ellipses were omitted from the calculation of the crystallization age (see supplementary section A2 for details).

A3 Geochronology of samples without zircon U-Pb data

A3.1 Samples 17FIN01, and 17FIN04A

Samples 17FIN01, and 17FIN04A are migmatites with medium-grained, garnet-bearing leucosome from the Turku area, Finland. In this area the crust was intruded by sediment-derived granites at ~1.85 Ga associated with high-temperature, low-pressure granulite facies metamorphism and migmatization (Huhma, 1986). We cite the age of 1850 Ma as the best estimate of the crystallization age of samples 17FIN01, and 17FIN04A. This is in accord with the ages obtained for four other samples from this area, ranging from 1815 ± 16 Ma to 1896 ± 26 Ma (see supplementary section A.1 for details).

A3.2 Sample 19GH3

Samples 19GH3, 19GH9, and 19GH11B are granites from felsic intrusions in the Baoulé-Mossi domain, West African Craton. The emplacement of felsic intrusions across the Baoulé-Mossi domain is associated with the 2.2-1.8 Eburnean Orogeny (Lompo, 2009). Parra-Avila et al. (2017) suggested that the ~2.3-2.0 Ga felsic magmatism in the Baoulé-Mossi domain migrated westward at a rate of 35 km/Myr. Sample 19GH3 was collected ~30 km southeast of sample 19GH9, and ~ 50 km east of sample 19GH11B. Given the close proximity of these

samples, we cite the ages of ~2.18 Ga obtained for samples 19GH9, and 19GH11B (see supplementary section A.1 for details) as the best estimate of the crystallization age of sample 19GH3.

A3.3 Sample SP-17-43

Sample SP-17-43 is a garnet-biotite-muscovite granite from the Wenasaga Lake batholith, Superior province. The Wenasaga Lake batholith belongs to a suite of strongly peraluminous granite plutons that intruded the metasedimentary English River Subprovince at ~2.7 Ga (Nitescu et al., 2006). These granite plutons are interpreted to be the result of the peak episode of a metamorphic event at 2691 Ma that resulted in migmatization and anatexis of the sediments from the English River Subprovince (Corfu et al., 1995). We cite the age of peak metamorphism at ~2.69 Ga (Corfu et al., 1995) as the best estimate for the crystallization age of sample SP-17-43.

A3.4 Sample SP-17-13

Sample SP-17-13 is a garnet-biotite granite from the Quetico belt, Superior province. From 2671 to 2652 Ma a major phase of felsic plutonism occurred in the metasedimentary Quetico belt (Percival, 1989). We therefor cite the age of 2660 ± 10 Ma as the best estimate of the crystallization age of sample SP-17-13.

A3.5 Samples SP-17-33, SP-17-38, SP-17-82, SP-17-71, and SP-17-50

Samples SP-17-33, SP-17-38, SP-17-82, SP-17-71, and SP-17-50 are from various sediment-derived intrusions (Medicine Lake batholith, Treelined Lake Complex, Allison Lake batholith, and Sharpe Lake batholith) in the Superior Province. Neoarchean sediment-derived granites are common in the Superior Province (Breaks et al., 2005). Their emplacement has been linked to the collision of Archean tectonic blocks between ~2.7 and 2.6 Ga (Percival et al., 2006; Yang et al., 2019). We therefore cite ~2.65 Ga as the best estimate of the crystallization ages of samples SP-17-33, SP-17-38, SP-17-82, SP-17-71, and SP-17-50.

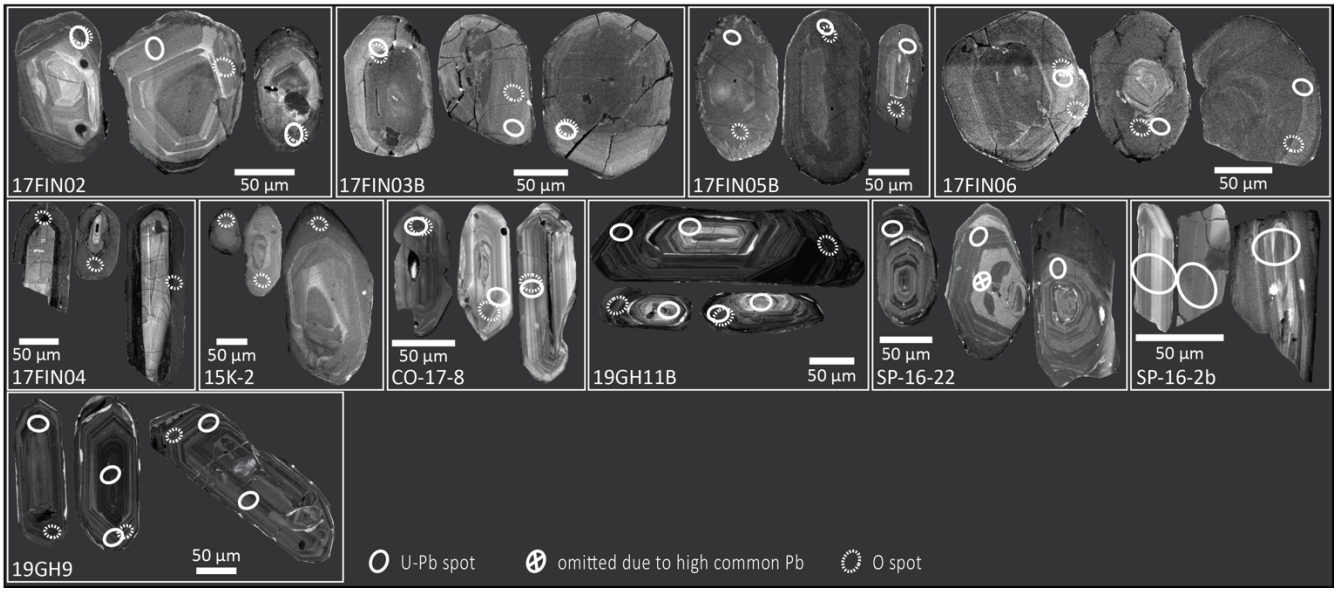

Supplementary Figure A2. Cathodoluminescence images of representative zircon grains with O and U-Pb spots marked.

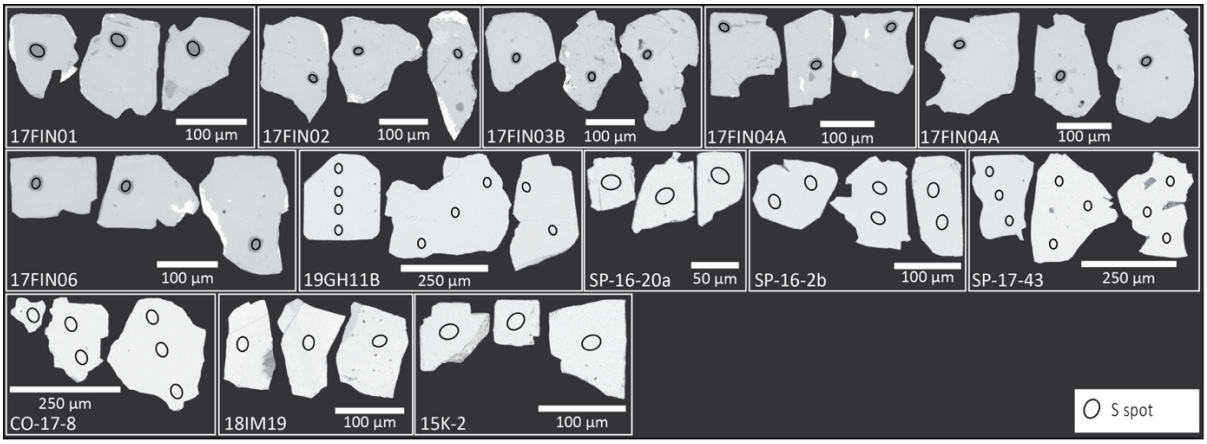

Supplementary Figure A3. Back scatter electron images of representative pyrite grains with S spots marked.

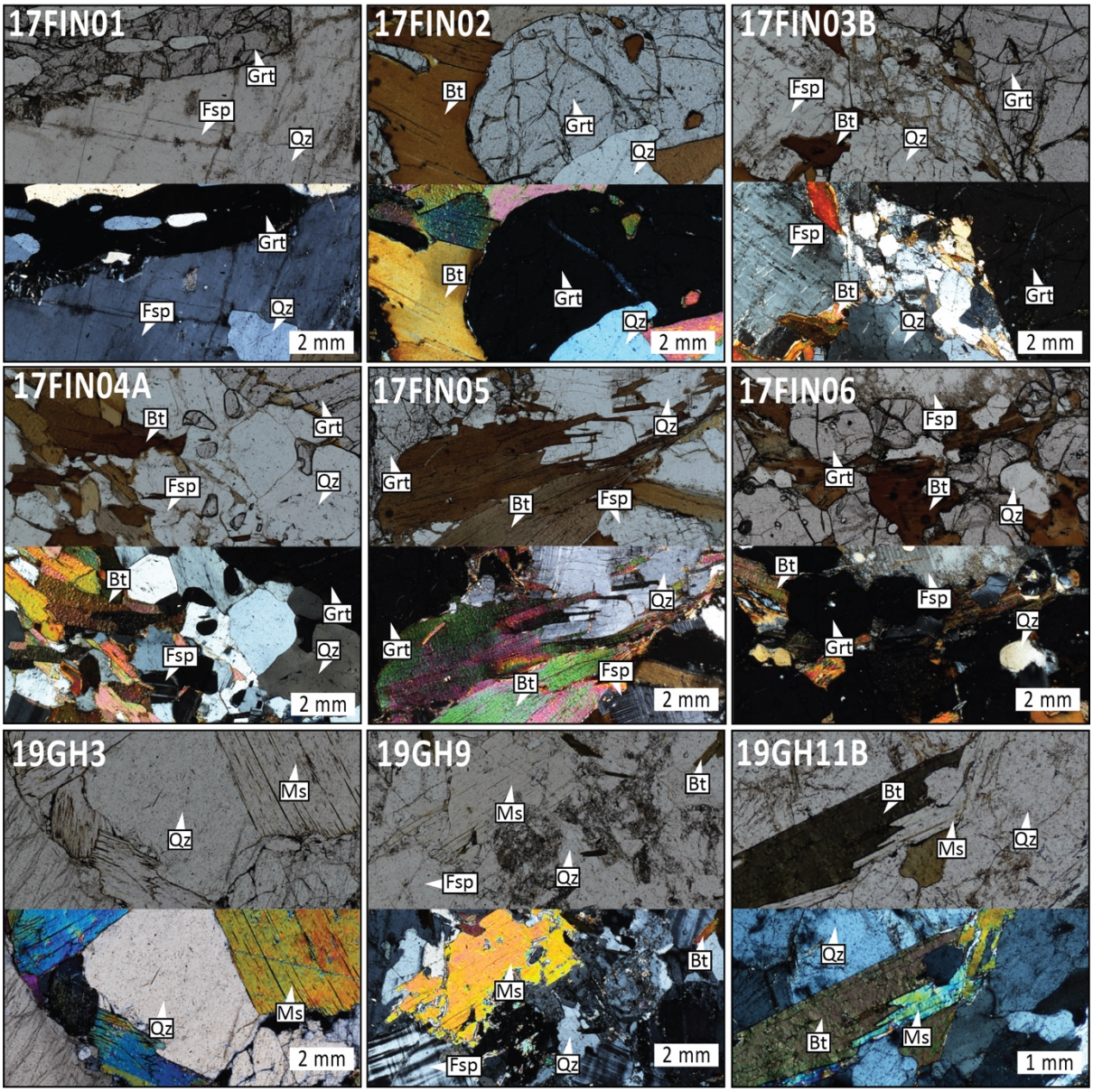

Supplementary Figure A4. Thin section photomicrographs. Mineral abbreviations: Qz, quartz; Fsp, feldspar; Grt, garnet; Ms, muscovite, Bt, biotite.

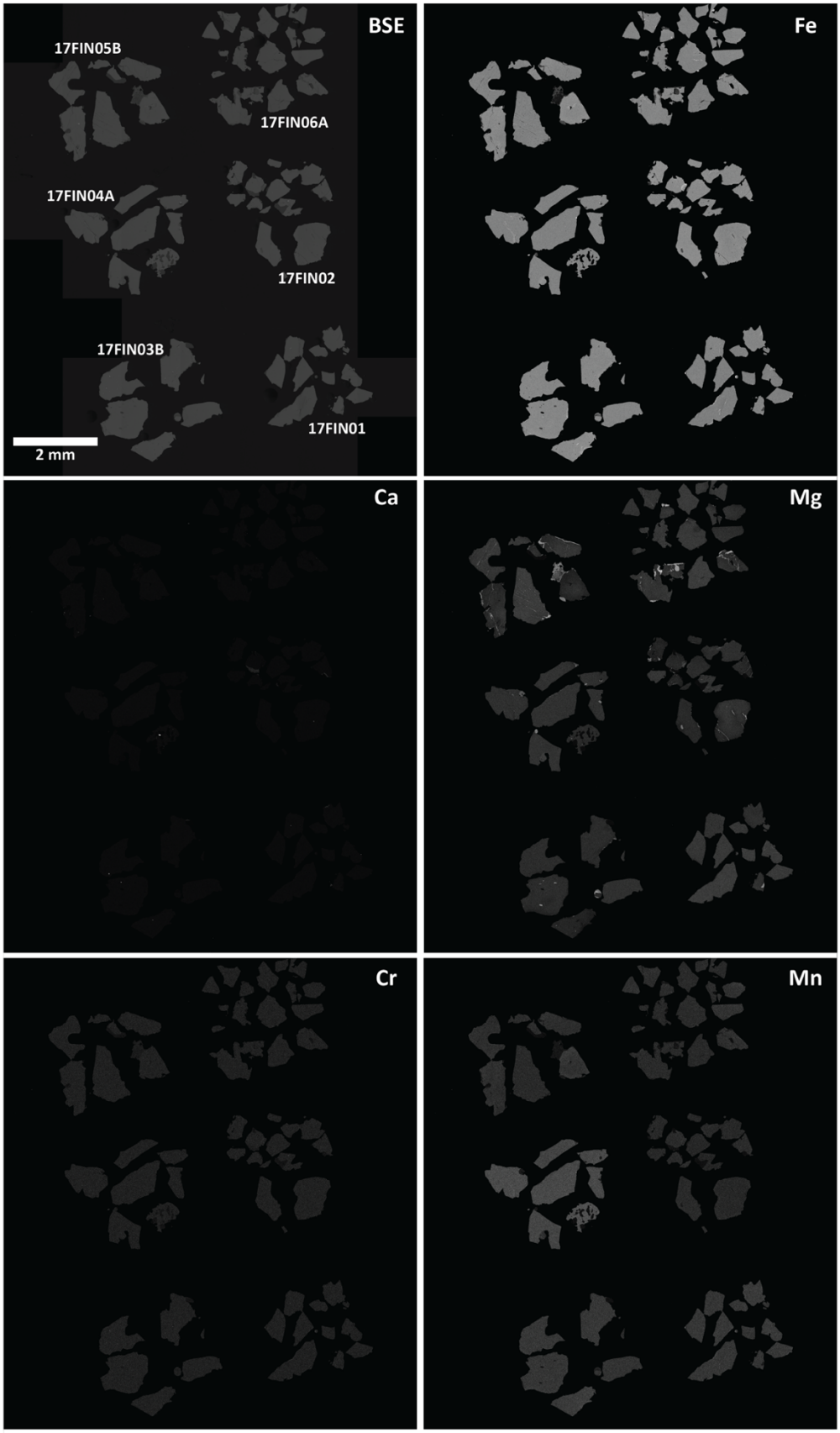

Supplementary Figure A5. Backscatter electron image and element maps of garnet in samples from the Baltic Shield, East European Craton. Garnet grains are Fe-rich, but Ca-poor indicating almandine rich garnet.

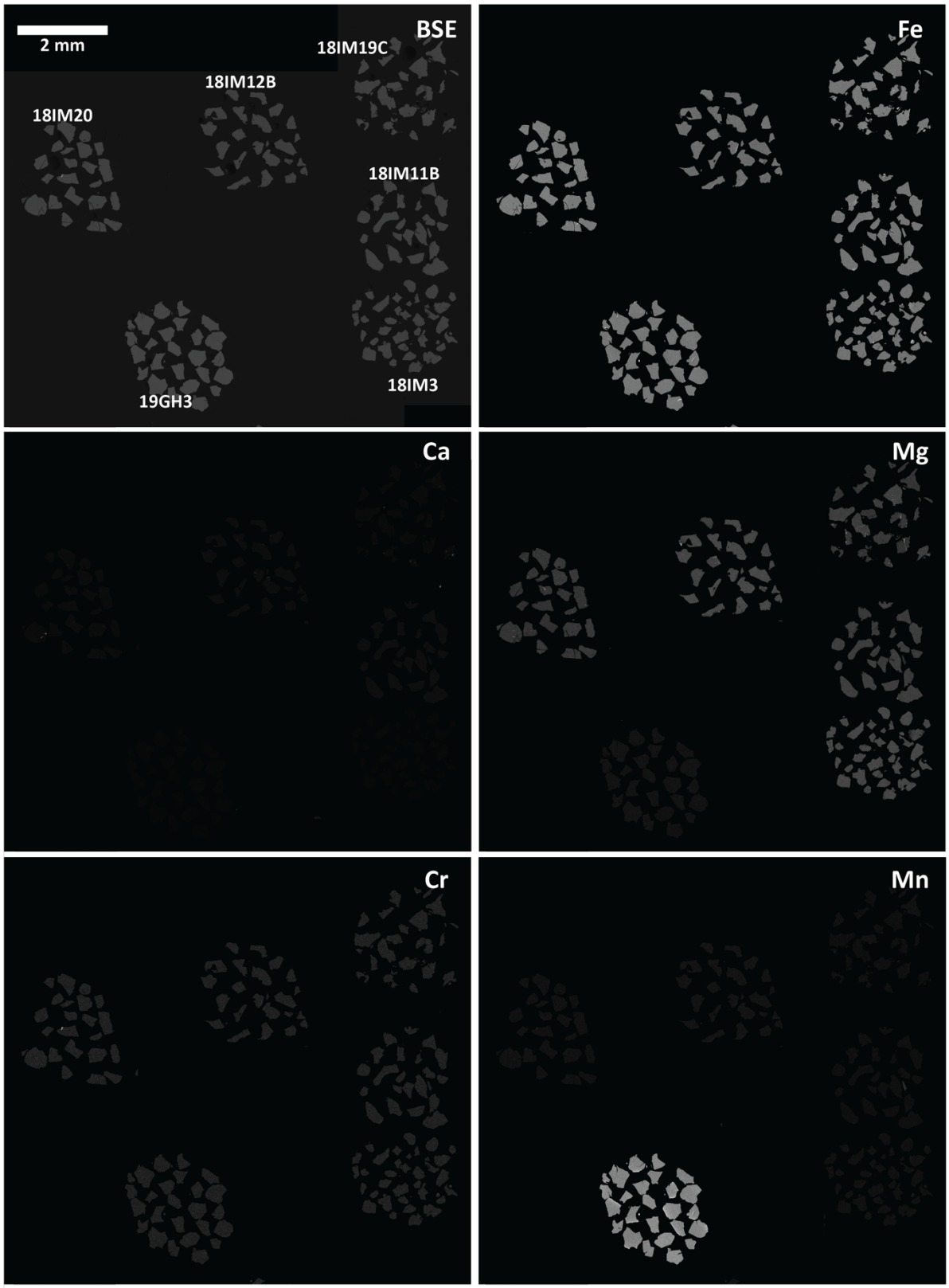

Supplementary Figure A6. Backscatter electron image and element maps of garnet in samples from the North China and West African Cratons. Garnet grains are Fe-rich, but Ca-poor indicating almandine rich garnet.

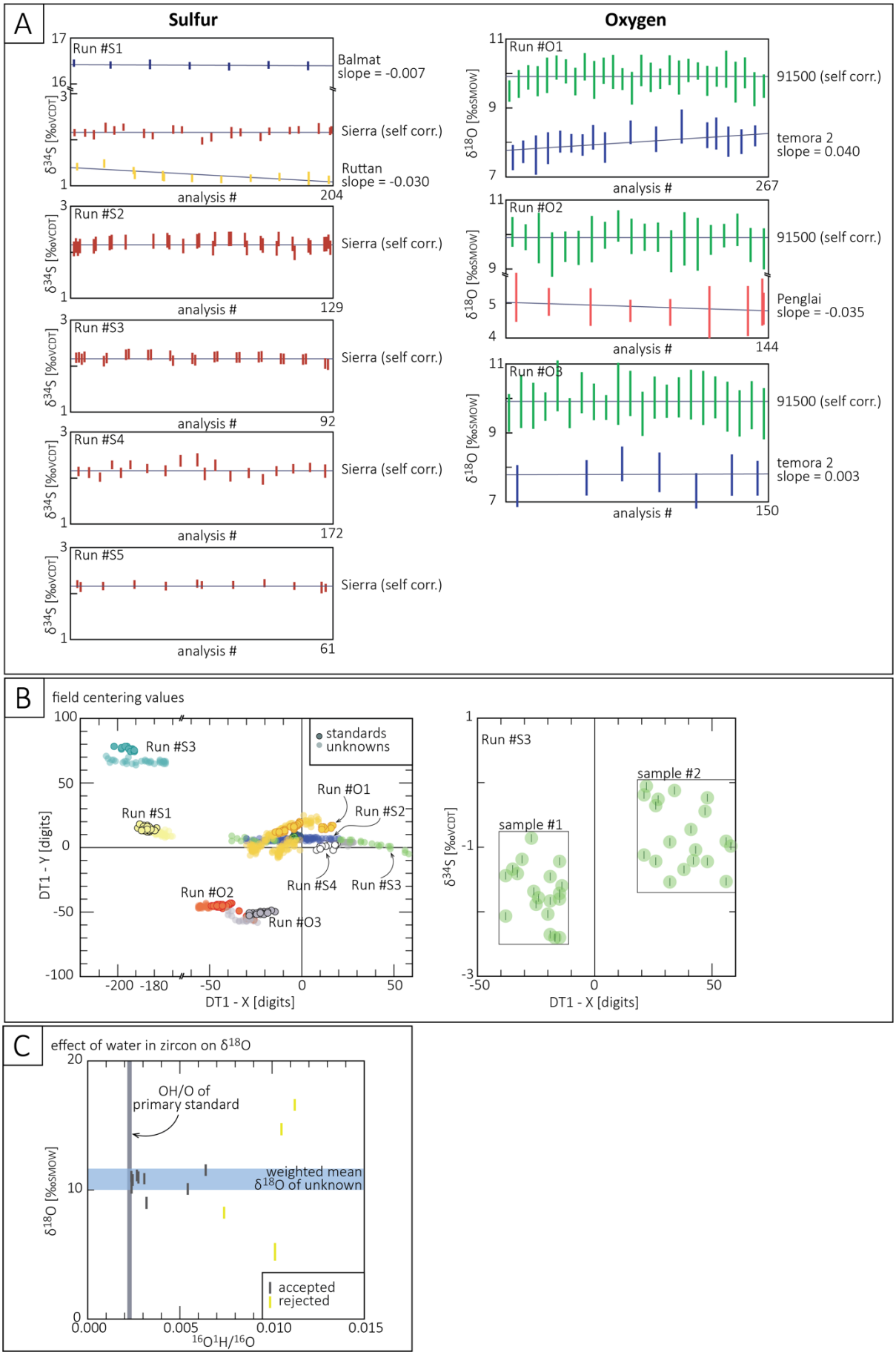
A
Sulfur
Oxygen
Run #S1
Balmat
slope = -0.007
Sierra (self corr.)
Ruttan
slope = -0.030
Run #S2
Run #S3
Run #S4
Run #S5
analysis #
204
129
92
172
61
δ34S [‰VCDT]
Run #O1
91500 (self corr.)
temora 2
slope = 0.040
Run #O2
Penglai
slope = -0.035
Run #O3
temora 2
slope = 0.003
267
144
150
δ18O [‰SMOW]
B
field centering values
standards
unknowns
DT1 - Y [digits]
DT1 - X [digits]
sample #1
sample #2
C
effect of water in zircon on δ18O
OH/O of
primary standard
weighted mean
δ18O of unknown
accepted
rejected
16O1H/16O

Supplementary Figure A7 (previous page). Sulfur and oxygen isotope data of standards and unknowns. (A) Corrected $\delta^{34}S$ and $\delta^{18}O$, respectively of standards over time show no significant drift. **(B)** Field centering values for standards and unknowns for each analytical run. Field centering (in X-direction) shows no correlation with measured isotopic composition, indicating that mount topography did not affect the analysis. **(C)** OH/O vs $\delta^{18}O$ plot. Measured $\delta^{18}O$ shifts with increasing zircon OH-content. Analyses with elevated OH/O (as compared to reference zircon) that yield distinctly lower or higher $\delta^{18}O$ values than those analyses with low OH/O are excluded from the calculation of the weighted mean $\delta^{18}O$ value.

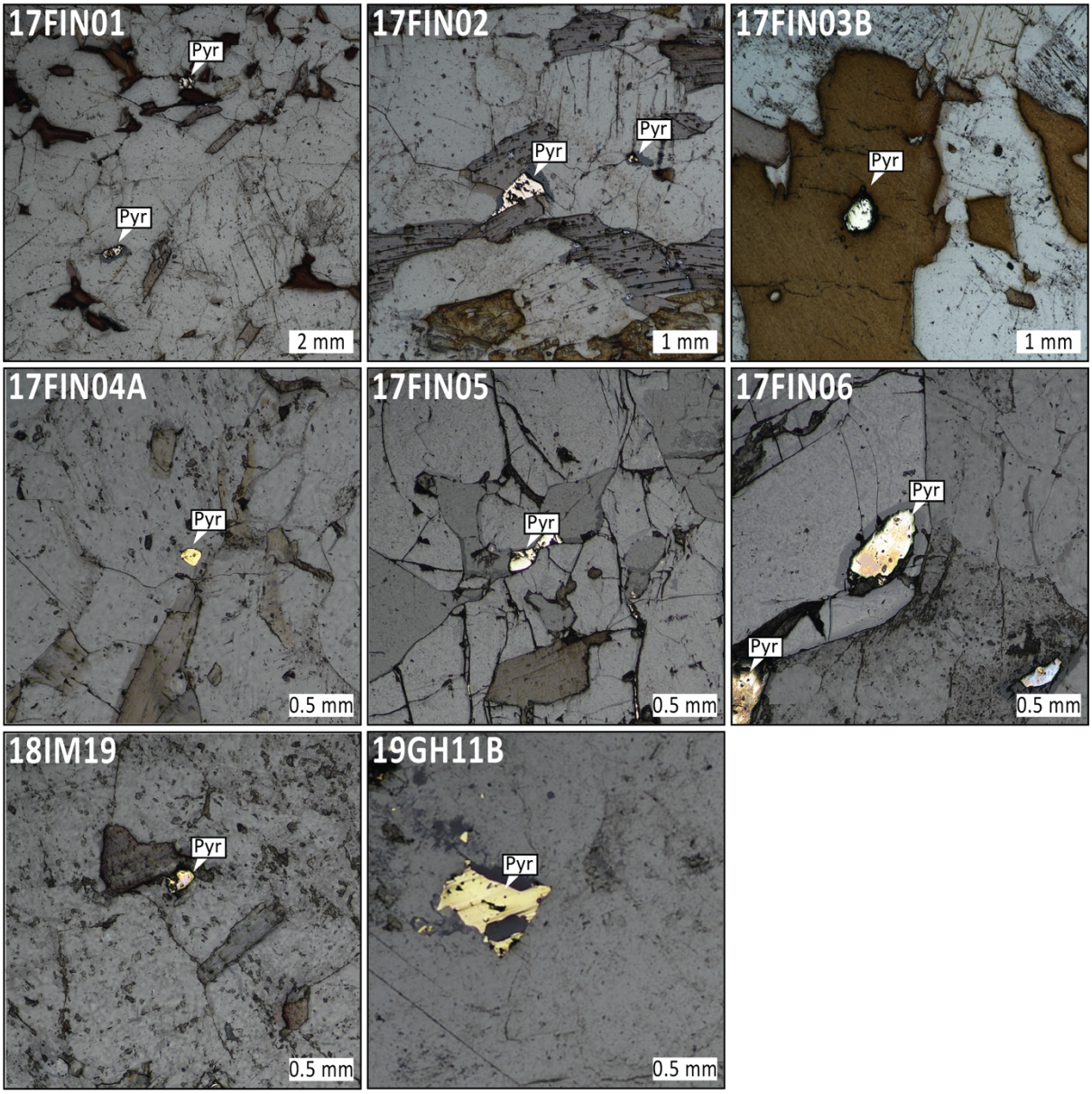

Supplementary Figure A8. Reflected light photomicrographs showing the occurrence of pyrite (Pyr) in thin section.

U-Pb (SIMS)	calibration standard		uncertainty/ reproducibility (1σ)		U concentration standard		secondary standard				
session #		# analyses	spot-to-spot	$^{238}U/^{206}Pb$* calibration		# analyses		# analyses	weighted mean age (Ma)	2σ	MSWD
U-Pb1	temora-2	13	1.50%	0.54%	temora-2	6	91500	5	1078 [1)]	31	0.68
U-Pb2	91500	5	0.50%	0.80%	OGC	4	OGC	4	3452 [2)]	35	0.6
U-Pb3	91500	10	0.50%	0.61%	OGC	6	OGC	6	3470 [2)]	13	0.47

Table A1. U-Pb measurement results of zircon reference materials for SIMS analytical runs. [1)] weighted mean $^{238}U/^{206}Pb$* age; [2)] weighted mean $^{207}Pb/^{206}Pb$* age.

U-Pb (LA-ICPMS)

Secondary standard	# analyses	weighted mean $^{238}U/^{206}Pb$ age (Ma)	2σ	MSWD	accepted age (Ma)	2σ	Reference
GJ1	16	601.00	2.00	0.73	601.20	0.40	(Jackson et al., 2004)
Plešovice	15	338.00	1.00	1.30	337.13	0.37	(Sláma et al., 2008)
91500	20	1062.00	2.00	1.30	1065.00	1.00	(Wiedenbeck et al., 2004)

Table A2. U-Pb measurement results of secondary zircon reference materials for LA-ICPMS analytical run.

O isotopes	primary standard				secondary standard			
session #		# analyses	$\delta^{18}O$	2σ		# analyses	$\delta^{18}O$	2σ
O1	91500	28	9.9	0.38	temora-2	17	8.0	0.48
O2	91500	20	9.9	0.41	Penglai	9	5.0	0.26
O3	91500	22	9.9	0.42	temora-2	7	7.8	0.42

Table A3. O isotope measurement results of zircon reference materials for SIMS analytical runs.

S isotopes	primary standard						secondary standards					
session #		# analyses	$\delta^{34}S$	2σ	$\Delta^{33}S$	2σ		# analyses	$\delta^{34}S$	2σ	$\Delta^{33}S$	2σ
S1	Sierra	22	2.17	0.15	-0.03	0.05	Balmat	10	16.34	0.24	-0.03	0.08
							Ruttan	10	1.24	0.25	-0.01	0.08
S2	Sierra	18	2.17	0.13	-0.03	0.08						
S3	Sierra	26	2.17	0.11	-0.03	0.07						
S4	Sierra	23	2.17	0.31	-0.03	0.06						
S5	Sierra	13	2.17	0.07	-0.03	0.06						

Table A4. S isotope measurement results of pyrite reference materials for SIMS analytical runs.

References

Breaks, F.W., Selway, J.B., and Tindle, A.G., 2005, Fertile Peraluminous Granites and Related Rare-Element Pegmatites, Superior Province of Ontario, *in* Short Course Notes, Geological Association of Canada 17, p. 87–125.

Corfu, F., Stott, G.M., and Breaks, F.W., 1995, U-Pb geoehronology and evolution of the English River Subprovince, an Archean low P-high T metasedimentary belt in the Superior Province: Tectonics, v. 14, p. 1220–1233, doi:10.1029/95TC01452.

Huhma, H., 1986, Sm-Nd, U-Pb, and Pb-Pb isotopic evidence for the origin of the early Proterozoic Svecokarelian crist in Finland: Geological Survey of Finland, 48 p.

Jackson, S.E., Pearson, N.J., Griffin, W.L., and Belousova, E.A., 2004, The application of laser ablation-inductively coupled plasma-mass spectrometry to in situ U–Pb zircon geochronology: Chemical Geology, v. 211, p. 47–69, doi:10.1016/j.chemgeo.2004.06.017.

Lompo, M., 2009, Geodynamic evolution of the 2.25-2.0 Ga Palaeoproterozoic magmatic rocks in the Man-Leo Shield of the West African Craton. A model of subsidence of an oceanic plateau: Geological Society, London, Special Publications, v. 323, p. 231–254, doi:10.1144/SP323.11.

Nitescu, B., Cruden, A., and Bailey, R., 2006, Integrated potential-field and seismic constraints on the structure of the Archean metasedimentary English River belt, Western Superior craton, Canada: Precambrian Research, v. 144, p. 261–277, doi:10.1016/j.precamres.2005.11.008.

Parra-Avila, L.A. et al., 2017, The geochronological evolution of the Paleoproterozoic Baoulé-Mossi domain of the Southern West African Craton: Precambrian Research, v. 300, p. 1–27, doi:10.1016/j.precamres.2017.07.036.

Percival, J.A., 1989, A regional perspective of the Quetico metasedimentary belt, Superior Province, Canada: Canadian Journal of Earth Sciences, v. 26, p. 677–693, doi:10.1139/e89-058.

Percival, J.A., Sanborn-Barrie, M., Skulski, T., Stott, G.M., Helmstaedt, H., and White, D.J., 2006, Tectonic evolution of the western Superior Province from NATMAP and Lithoprobe studies: Canadian Journal of Earth Sciences, v. 43, p. 1085–1117, doi:10.1139/e06-062.

Sláma, J. et al., 2008, Plešovice zircon — A new natural reference material for U–Pb and Hf isotopic microanalysis: Chemical Geology, v. 249, p. 1–35, doi:10.1016/j.chemgeo.2007.11.005.

Wiedenbeck, M. et al., 2004, Further characterisation of the 91500 zircon crystal: Geostandards and Geoanalytical Research, v. 28, p. 9–39, doi:10.1111/j.1751-908X.2004.tb01041.x.

Yang, X.-M., Drayson, D., and Polat, A., 2019, S-type granites in the western Superior Province: a marker of Archean collision zones: Canadian Journal of Earth Sciences, v. 56, p. 1409–1436, doi:10.1139/cjes-2018-0056.